Pamukkale Üniversitesi Mühendislik Bilimleri Dergisi
Pamukkale University Journal of Engineering Sciences

Çift fazlı çeliklerin nokta direnç kaynağı ile birleştirilmesinde akım etkisi

The effect of current on the resistance spot welding of dual phase steels

Mesut ÖZER[1], Ali KİBAR[2], Mehmet UÇAR[1]*

[1]Department of Automotive Engineering, Kocaeli University, Kocaeli, Turkey.
mesut.ozer@kocaeli.edu.tr, ucarm@kocaeli.edu.tr
[2]Department of Mechanical and Material Technologies, Kocaeli University, Kocaeli, Turkey.
alikibar@kocaeli.edu.tr

Received/Geliş Tarihi: 12.04.2023 Revision/Düzeltme Tarihi: 03.09.2023 doi: 10.5505/pajes.2023.13704
Accepted/Kabul Tarihi: 23.09.2023 Research Article/Araştırma Makalesi

Abstract

Nokta direnç kaynaklı birleştrimelerdeki akım değerinin mekanik ve metalurjik özellikler üzerindeki etkisi galvanizli farklı kalınlıklardaki DP600 çelik saclar kullanılarak deneysel olarak incelenmiştir. Numuneler 1.5 ve 1.8 mm kalınlıklarda seçildi. Kaynak proses parametreleri, 5 kN elektrod kuvveti, 7, 9, 11, 13, 15 kA kaynak akım değerleri,180, 240, 300, 360 ve 420 ms kaynak süreleri tercih edilerek gerçekleştirilmiştir. Kaynak birleştirmeli numuneler, en yüksek çekme mukavemetinin belirlenmesi için çekme-makaslama testine tabi tutuldu. Optimal numuneler optik mikroskop ve taramalı electron mikroskobu ile incelendi. Nokta kaynağı değişkenlerinin maksimum dayanım üzerindeki etkisi belirlendi, akım-süre değerlerini gösteren lobe diyagramı elde edildi. Optimum kaynak parametreleri yeni saclarda başarıyla uygulandı. Deneysel sonuçlar gösterdi ki; kaynak akımı özellikle çarpışma enerjisi emiliminde ve yük taşıma kapasitesinde önemli bir rol oynamaktadır.

Anahtar kelimeler: Otomotiv gövde, Çift fazlı çelik, Enerji emme kapasitesi, Nokta direnç kaynağı, Kaynak hata tipleri

Öz

The effect of current on resistance spot welding joints on metallurgic and mechanical properties is investigated experimentally using galvanized unequal-thickness DP600 steel sheets. The specimens were chosen to be 1.5 and 1.8 mm thicknesses. The parameters of the welding process were preferred as an electrode force at 5 kN, welding currents at 7, 9, 11, 13 and 15 kA and welding times at 180, 240, 300, 360 and 420 ms. The welded joint specimens were subject to tensile-shear strength testing to determine the ultimate tensile strength. Optimal specimens were inspected using optical microscopes and scanning electron microscopy. The effect of spot welding variables on the ultimate tensile strength was determined and the lobe diagram, which shows optimal current-time values, was obtained. The optimal welding parameters were carried out on new sheet metals successfully. The experimental results show that the welding current plays an important role in the especially crash energy absorption and load-carrying capability.

Keywords: Automotive body, Dual phase steel, Energy absorption capability, Resistance spot welding, Weld failure types

1 Introduction

Advanced high-strength steels are usually chosen by vehicle factories due to their ability to achieve high strength, enhanced vehicle safety, reduced vehicle weight, high corrosion resistance and high crash performance. One of the most common AHSS steel types is dual-phase (DP) steel in the automotive industry [1]. DP steels consist of two phases: hard martensitic and ductile ferrite. A hard martensitic second phase is surrounded by a ductile ferritic matrix first phase [2]. DP steels have good formability and a high energy absorption capacity compared to conventional high-strength low-alloy (HSLA) steels of equal strength. The use of DP steels, especially in vehicle production, requires an investigation of the joining abilities of these steels [3]. Resistance spot welding (RSW) is a common metal welding process to join automotive parts in non-detachable joints. Although the spot weld quality index is an important issue, the mechanical, electrical, and thermal properties of steel alloys make RSW more difficult to perform [4].

It is necessary to know the parameters affecting the amount of heat required for the formation of the weld nugget to obtain the desired quality index and the maximum load-carrying value in spot resistance welding. The amount of heat required for the formation of the weld nugget depends on three factors. The heat energy is directly proportional to the conductor resistance and the application time of the current, while it is directly proportional to the square of the current, as given in Equation (1).

$$Q = I^2Rt \quad (1)$$

Where Q = heat, joules; I = current, amperes; R = resistance, ohms; t = duration of current, seconds.

In the case of RSW, the types of failure observed as a result of the tensile shear test gives us a clue about qualitative measures of welded joint quality [5]. That is, this failure type of RSW is a qualitative measure of the joining quality. When a tensile shear test is conducted on welded joints, failure can happen in three distinct weld zones: the base metal (BM), heat-affected zone (HAZ) and fusion zone (FZ) [6]. There are various welding failures in RSW. As shown in Figure 1, interface failure (IF) and pullout failure (PF) occur if the joining is broken at FZ and HAZ or BM, respectively [7].

Tensile shear tests are used to determine how residual stress, which affects the mechanical properties of the welded joint, is affected by process variables such as current, welding time and electrode pressure force. The welding failure types are directly determined by these parameters. The welding parameters relating to current, and time were investigated by Sung [8] and Zhang [9]. They stated that while a long welding time or high

*Corresponding author/Yazışılan Yazar

Table 1. Chemical composition of DP600 (wt.%)

Material	C	Cr	P	Mn	Al	Ni	Co	Si	S	Nb	Fe
DP600	0.135	0.02	0.01	1.5	0.04	0.039	0.019	0.2	0.004	0.015	Base

Table 2. Mechanical properties of DP600

Specimen	YTS (N/mm2)	TS (N/mm2)	% Elongation	Hardness (HV)
DP 600	345	625	25	286

welding current might cause excessive expulsions (EE), a short welding time or low welding current might cause cold welds (CW) or undersize welds (UW). Such events are undesirable and should always be avoided since they mean an insufficient penetration rate. However, Zhou and Cai investigated theoretically and experimentally the effect of electrode force on the RSW process and demonstrated that large electrode forces cause short welding times [10]. Therefore, the optimum welding current and time should be selected for an optimum welding schedule in a welding process [11].

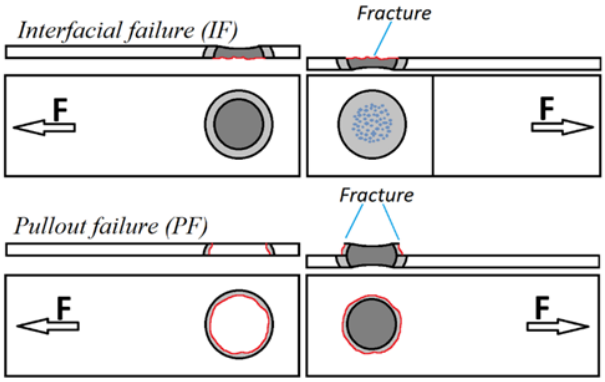

Figure 1. Fracture in IF-PF mode failure types.

The weld current-time lobe diagram is obtained in the present study to evaluate the impact of weld current on the weld quality index. The weldability regions in this diagram are obtained and those current-time values are examined to find the best-quality joints [12]. The microstructures of the joints attained by different welding currents are compared. In that way, an experimental study will be put forward on the joining sheet metals with various thicknesses for automobiles. According to the data of the ULSAB-AVC Program [13], DP steels are mainly used in passenger-type vehicle constructions. Since different thicknesses of DP sheet metal are combined in different chassis regions, this experimental study will shed light on such joining processes.

2 Experimental study

In this experimental study, zinc-coated (galvanized) DP600 steel was used as a BM sheet. The chemical material composition and mechanical mechanism with a Programmable Logic Controller (PLC) controlled single lever. Welding processes were conducted using a dome-type electrode 6 mm in diameter. Figure 2 shows the test specimen dimensions prepared for the experimental properties of galvanized DP600 steel are given in Tables 1 and 2. The welded samples were obtained by mating and welding sheets in 1.5 and 1.8 mm thicknesses. The RSW process was performed using a 150 kVA capacity and 50 Hz frequency pedestal type RSW machine, which had a pneumatic. Welding was performed by overlapping the ends of both sheet materials by 30 mm.

A tensile shear universal testing device performed the tensile test on the specimens at a crosshead speed of 20 mm/min. In order to deduct the peak load and failure, the load-displacement curve was applied. The deformed and failed samples were used to determine the failure mode. Optical microscopy and an Inspect S50 scanning electron microscope (SEM) were used to analyze the FZ and HAZ microstructures of unequal weld joints. A microhardness test device (Shimadzu HMV-2T) was used to determine the hardness state of HAZ, BM and FZ using a 500 g load.

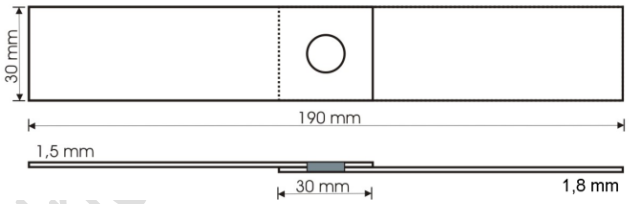

Figure 2. Tensile–shear test sample dimensions.

The effects of different conditions on welding performance were examined using a total of 25 welding schedules. Three samples were tested for each parameter. The electrode force was kept constant at 5 kN and chosen depending on the thickness of the BM. The welding currents were incrementally increased by 2 kA from 7 to 15 kA, and the welding times were incrementally increased by 60 ms from 180 to 420 ms to study these effects of welding parameters. A preheating step was necessary to decrease the effect of surface conditions such as coating effects, contamination and roughness, etc. In this step, 4 kA welding current, 2.5 kN force, and 280 ms time were used as preheating variations. The minimum and maximum weld currents were determined to be between 7kA and 15kA, respectively, with weld times ranging from 180ms to 360ms.

3 Results and discussion

In this experimental study, the mechanical behaviours are quantitatively evaluated by tensile shear tests after welding all specimens with specified parameters. The result of the tensile shear test on a specimen and its failure type is affected by the changes in welding time and current. At the end of the tests, the following results were observed;

As seen in samples 1-5, if the welding current is too low, there is not enough heat input to form a weld nugget, which results in unformed weld nugget, it is called Cold Weld (CW). It is clear from these experiments that; If the welding current is insufficient, the welding time magnitude is irrelevant. This type of spot weld is not expected to carry loads.

In samples 6-7, In that case, IF mode occurs as a failure type. The crack propagated through the nugget. It indicates the weld nugget did not form enough to withstand the high peak load.

Table 3. Welding parameters, peak loads, failure types and indentation rates of DP600.

Experiment Number	Welding Current (kA)	Welding Time (ms)	Tensile Load (N)	Failure	% Indentation
1	7	180		CW	
2	7	240		CW	
3	7	300		CW	
4	7	360		CW	
5	7	420		CW	
6	9	180	669,6	IF-CW	0,9
7	9	240	1736,7	IF-CW	1,5
8	9	300	2242,4	PF	2,7
9	9	360	2407,3	PF	3,6
10	9	420	2463,7	PF	7,3
11	11	180	2349,0	PF	4,2
12	11	240	2470,0	PF	14,8
13	11	300	3017,3	PF	19,4
14	11	360	2597,7	PF	17,3
15	11	420	2605,4	PF	17,3
16	13	180	2231,6	PF	36,4
17	13	240	2299,7	PF	21,2
18	13	300	2517,2	PF	34,8
19	13	360	2185,3	PF	28,2
20	13	420	2303,1	PF	30,0
21	15	180	2321,6	PF	32,7
22	15	240	2382,7	PF	36,4
23	15	300	2442,0	PF	31,2
24	15	360		EE	
25	15	420		EE	

This has a deleterious effect on the crash performance of vehicles, as there is almost no plastic deformation in the IF mode. Most of the spot welds have pores on the FZ fracture surfaces [14]. However, the increase in the welding time had a positive effect on the load carrying amount.

In samples 8-23, after the tensile shear test, pullout fracture defects are observed. By raising the welding current, it is possible to see the transition from IF to PF failure types. PF is a desirable type of weld failure. The data in the table 3 are more clearly shown in the graph in Figure 3.

In samples 24-25, Excessive expulsion has occurred. As mentioned earlier, excessive welding time and welding current cause excessive expulsion, this causes material loss in the weld zone. So the process results in reduced peak load and energy absorption.

The maximum tensile strengths corresponding to the parameters and the weld indentation rates, which are due to the pressure of the electrodes on the melt, are presented. Indentation values exceeding 30% do not comply with AWS D8.7 standards [15]. Therefore, none of the samples joined with a current value of 15 kA are suitable. The best load-carrying capacity is obtained in welds with 11 kA and 13 kA currents, respectively. The weld's load-carrying capability at a current of 9 kA rises with an increase in welding time.

Therefore, welding at a low welding time is not suitable for this current value. Although load-carrying values are high in welding at 15 kA current, they are not acceptable welds due to surface conditions (indentation). The most ideal RSW welding is 11 kA current and 300 ms time. Figure 4 shows the lobe graph of weldable parameter regions, obtained according to the welding parameters by keeping the electrode pressure force at 5 kN [16].

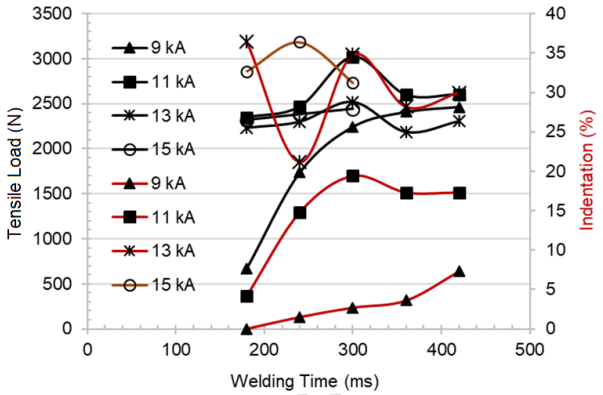

Figure 3. Time, strength and indentation graphic. The black and red lines show the tensile strength of the samples and the indentation rate, respectively.

The welding lobe chart is the weld current and time chart, which shows the parameters of the ideal welding spots after the tensile shear test. Square dots in this lobe graph show the region where the weld current and time are insufficient. Welding penetration is low and load-carrying capability is insufficient, especially in welding with 7 kA current and 9 kA with 180, 240 ms times. Generally, welding performed with 11 and 13 kA welding currents shows the most efficient joints. The experiment with 11 kA, 300ms parameter was repeated three times under the same conditions. The amount of deviation in the load carrying capacity was found as ± 110 N. As the welding time and current increase, expulsion occurs in the welding and causes uneven load-carrying values and poor surface quality, resulting in material loss from the welding area. Excessive expulsion occurs in the joints at 15kA and 360-420 ms welding conditions. These regions are shown in triangle dots in the lobe chart, as shown in Figure 4.

As seen in Figure 4, 7 kA welding current is not enough to melt the base metal, which results in CW. The base metal starts to melt at a current of 9 kA and a time of 180 ms. In this case, an IF occurs between welded sheet metals. Additionally, the most ideal nugget formation occurs at 11-13kA current values. At higher currents, expulsion occurs, and the welded joint's bearing capability is reduced.

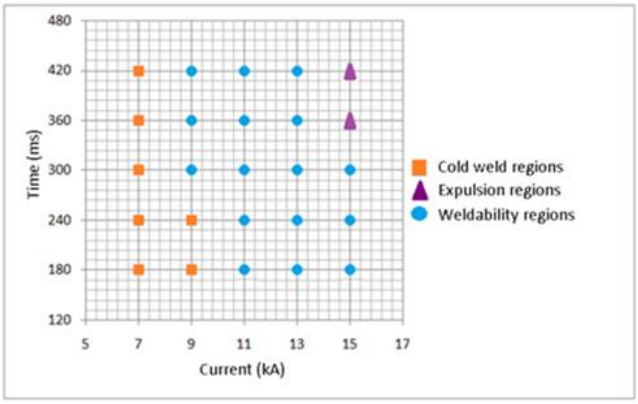

Figure 4. Lobe graphic of RSW.

The magnitude of the weld tensile energy is one of the indicators of crash performance. The mechanical performance of a joint can be evaluated with regard to energy absorption (EA) and peak load, as well as failure modes. Spot welds have a maximum capacity known as EA to absorb the energy of an impact load during a mechanical occurrence like a car collision. The maximum displacement indicates the degree of ductility of the welded joint and, therefore, the impact absorption performance [17].

Zhang and Senkara [15] expressed the magnitude of the measured area under the peak of the curve in the load-elongation diagram. The PF has a larger peak load and better energy absorption, but the IF is excessively brittle, has a lower peak load, weaker strength, and is less ductile. The load-displacement of typical failure modes of IF-CW, PF and EE are shown in Figure 5.

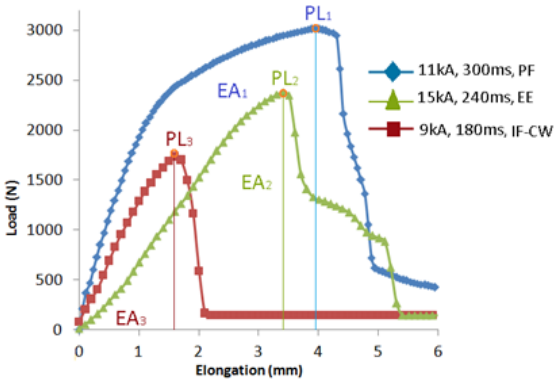

Figure 5. The specimens' amount of energy absorption and peak load graphic.

PF is more ductile, has a higher peak load and also absorbs more deformation energy within 11 kA current and 300 ms time, compared to PL_1. However, the maximum crash energy absorption is obtained in the PF specimen. The increase in current by 15 kA causes expulsion, even if the time is short. It can be seen in the graph that the impact absorption performance decreased in this welded joint. The lowest impact absorption performance is realized at 9 kA current and 180 ms, where the low penetration occurs due to insufficient current value. As the time and current parameters increase up to the expulsion level, the nugget diameter will also increase. Apart from the optimum energy absorption, high indentation rates also reduce the absorption performance.

As a result of the destructive inspection of the tensile test, IF and PF welding failures welded and fractured regions are shown in Figure 6. The ideal welding sample bearing a static load of 3,017 N is shown in Figures 6 b-e-h. Insufficient current causes low weld penetration and inability to provide sufficient strength, as shown in Figures 6 a-d-g. Excess welding time/current has an adverse effect on the spot, causing expulsion and surface indentation, as shown in Figures 6 c-f-i.

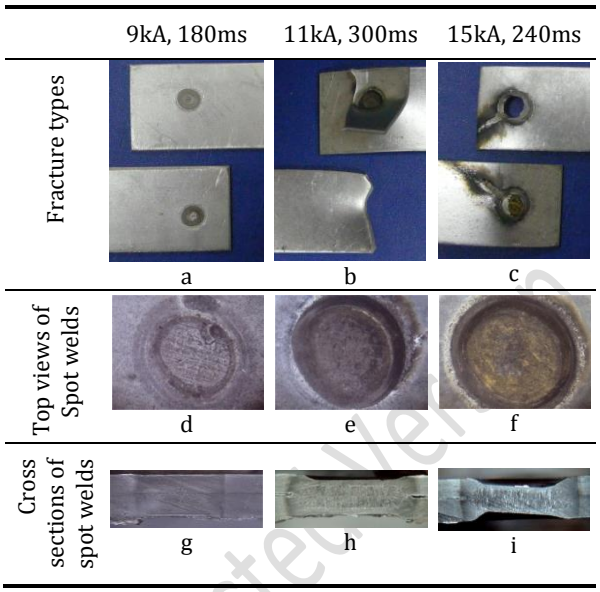

Figure 6. Several failure types after tensile–shear tests. Weld current and time values.

4 Microstructure and hardness characteristics

The cross-sectional macrostructure of an RSW joint of unequal DP600 joints viewed by optical microscopy is shown in Figure 7. It is performed at 11 kA current and a time of 300 ms. The final solidification line is placed at the centre of the entire thickness of sheet metal matches, shown as region (b). The current effects on the specimens are performed with 7, 9, 11, 13 and 15 kA currents and inspected 11, 13, and 15 kA performed specimens by SEM.

The welded joint is composed of several zones, namely the HAZ and FZ, shown as (a) and (b) in Figure 8, respectively. Different regions are separated by distinct boundaries. Melting metal is used to solidify the FZ while it is rapidly cooling. The greatest cooling rate reportedly approaches 1200°C/s according to report by Alizadeh et al [18]. The solidification line of the weld nugget, which has an unequal thickness, is placed at the centre of the BM's total thickness. The formation of the weld nugget is influenced by thermal conductivity and electrical resistance, which regulate heat generation and dissipation. The differences in the electrical resistance and thermal conductivity of two steel sheets cause an asymmetrical weld nugget to form at the unequal metal joints. However, a symmetrical nugget is formed during the welding of two DP600 sheets with equal thickness, as shown in Figure 8. It is also noteworthy that fracture propagation of unequal thickness DP steels is located in the HAZ of the thinner sheet. It also occurs along the ferrite–martensite interfaces.

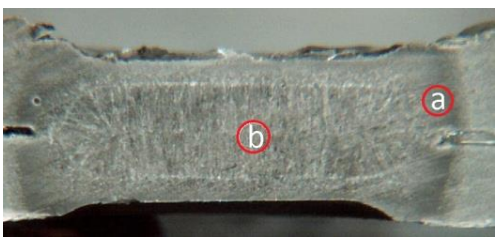

Figure 7. The cross-section of the resistance spot welded the joint of the unequal DP600 joint.

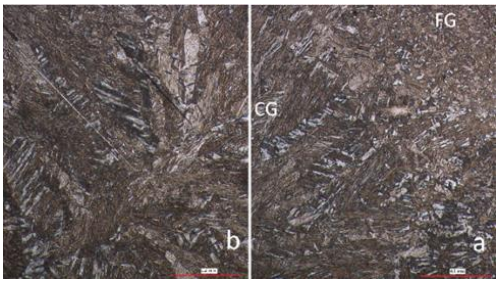

Figure 8. Optical microscope image of the cross-section of an RSW joint of the DP600 joint.

Figure 9 shows the microstructure of the weld joints for different zones. There are two types of zones in the images, light and dark. The most needle-like martensite (light zone) is dispersed in a ferrite (dark zone) matrix. The microstructures vary clearly from the BM to the nugget, and the grains in the HAZ change from coarse-grained to fine-grained type as the distance from the spot weld centre increases [19,20]. The maximum temperature reached in the FG HAZ surpasses the Ac3 temperature threshold and is maintained only for a brief period, which restricts the growth of grains [21]. Conversely, the peak temperature in the CG HAZ also exceeds Ac3, but it persists for a longer duration, allowing more time for the austenite grains to coarsen compared to those in the FG HAZ. In other words, the CG HAZ experiences prolonged exposure to high temperatures, leading to more significant growth of the grains than in the FG HAZ. The fusion zones in Figure 9 show structures formed by welding currents of 11, 13, and 15 kA (top to bottom), all of which are dominated by columnar grains. High-temperature gradients are caused by the fast-cooling rate, which also determines the volume of martensite [9]. It seems that the most intensive martensite volume distribution in different zones of a weld joint is in the fusion zone at 15kA.

Ferrite and lath martensite HAZ zones are integrated with the microstructure of the DP600 HAZ zones in the case of 11-13kA range. 15 kA HAZ demonstrates a heavily tempered martensite structure. The martensite volume ratio increases in the order of FZ and HAZ by an increase in the weld current, as shown in Figure 9. It is necessary to know the hardness in the BM, FZ and HAZ regions to understand the changes in the microstructure. For this, the hardness is measured along the diagonal traverse line in the weld section. In terms of weld hardness, the CG HAZ has the lowest hardness (190 HV) out of all the weld zones. This causes PF failure during tensile–shear testing. FZ zones have the highest hardness ratio with 375 HV among all the weld zones (Figure 10).

Hardness values close to each other are measured in three samples welded at a time of 300ms and a current of 11,13,15 kA. (Fig. 10). However, there is nearly twice the difference in hardness between the FZ and the HAZ. Due to the rapid cooling of the welding electrodes, the FZ zone is hard, rigid and robust, while the slowly cooling HAZ region, where the welding electrodes do not come into contact, has a softer grain structure. Therefore, the region where the initiated fracture will start during the tensile test is the HAZ. FZ hardness is used to control the joints' mechanical properties in the IF mode. The hardness of the HAZ is used to control the tensile–shear peak load of the joint in the PF mode [22].

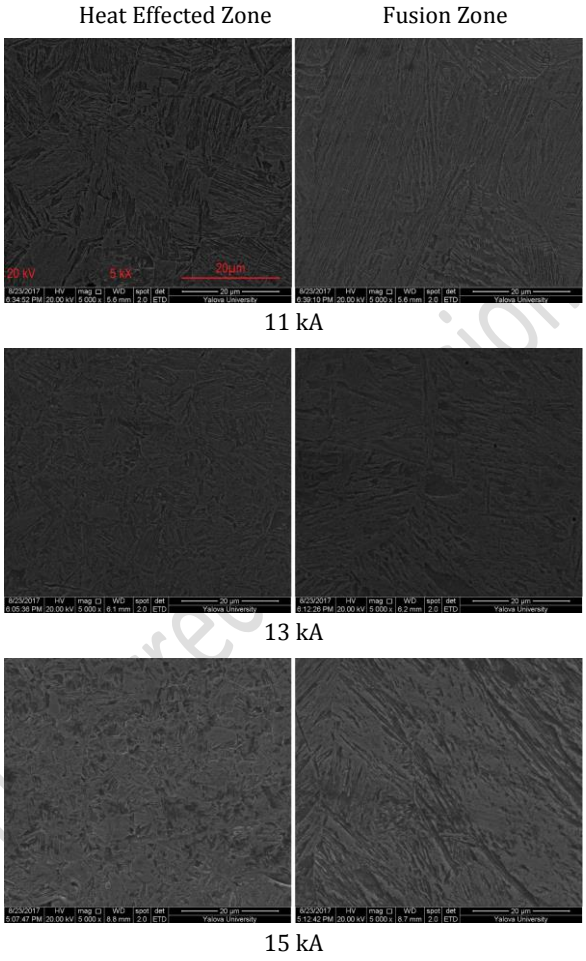

Figure 9. SEM views.

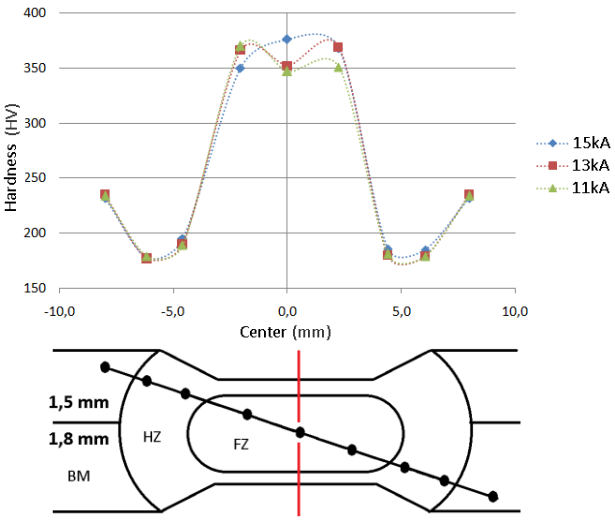

Figure 10. Hardness characteristics of an optimal specimen.

5 Conclusion

The effect of welding current/time on the mechanical properties and microstructures of welding joints for galvanized DP600 sheet metals were investigated experimentally using tensile shear tests, inspections using optical and SEM

microscopes, and hardness value. The results indicate that spot welding's ability to absorb energy and carry loads during tensile-shear tests is significantly impacted by the welding current. The capability of energy absorption is a significant factor in vehicle crash worthiness. The failure of energy and peak-load levels of unequal joints increase as the welding current increases until expulsion failure occurs. The static tensile-shear test revealed interfacial and pullout fractures as distinct failure mechanisms. Increasing the welding current causes the interfacial mode to change into the pullout mode. On the other hand, if the welding current is increased too much, there might be significant expulsion and indentation. The critical welding current is determined to be between 11 and 13 kA. Furthermore, the microstructure of the welding zones is found in the CG HAZ region. An 11 kA to 13 kA welding current is the optimal degree for quality joints. If the amount of current increases, the CG HAZ changes to a heavily tempered soft structure, which negatively affects peak-load values.

However, not only the welding current has an effect on the nugget formation, but also how important the welding time is in terms of the formation of the welding nugget and increasing the load carrying capacity. Insufficient welding time can lead to cold welding, resulting in undesirable welds. Increased welding time improves load-carrying capacity and performance. However, excessive time can cause expulsion and material loss, reducing peak load and energy absorption. The ideal welding parameters are 11 kA current and 300 ms time, resulting in desirable mechanical behaviours.

6 Author's Contributions

In the scope of this study; the project idea was formulated by authors 1 and 3. Author 1 was responsible for drafting and writing the manuscript, conducting the experiments, and analysing the results. Author 3 contributed by providing analytical insights on the structural aspects, supervising the experiment's progress, interpreting the results, and assisting in the preparation of the manuscript. Similarly, author 2 also provided analytical insights on the structural aspects, supervised the experiment's progress, evaluated the findings, and assisted in writing the article.

7 Ethics

Ethics committee permission is not required for the article prepared. There is no conflict of interest with any person/institution in the article prepared.

8 References

[1] Hayat F, Sevim İ. "The effect of welding parameters on fracture toughness of resistance spot-welded galvanized DP600 automotive steel sheets" *The International Journal of Advanced Manufacturing Technology*, 58:1043–1050, 2011
Doi: http://dx.doi.org/10.1007/s00170-011-3428-x

[2] Wang W, Wei X. "The effect of martensite volume and distribution on shear fracture propagation of 600 – 1000 mpa dual phase sheet steels in the process of deep drawing" *International Journal of Mechanical Sciences*, vol. 67 pp. 100–107, 2013
Doi: http://dx.doi.org/10.1016/j.ijmecsci.2012.12.011

[3] Ramazani A, Abbasi M, Prahl U, Bleck W. "Failure analysis of DP600 steel during the cross-die test", *Computational Materials Science*, vol. 64, pp. 101–105, 2012.
Doi: http://dx.doi.org/10.1016/j.commatsci.2012.01.031

[4] Rashid M, Medley JB, Zhou Y. "Electrode worksheet interface behaviour during resistance spot welding of al alloy" *Science and Technology of Welding and Joining* vol. 14, no. 4, pp. 595–604, 2009.
Doi: 10.1179/136217109X406947

[5] Demir B., Elitas, M., Karakuş H.. "Nokta direnç kaynağı ile birleştirilen DP600 çeliğinin çekme makaslama özelliğinin incelenmesi" *Pamukkale Univ Muh Bilim Derg*. 2022; 28(4): 533-538 Doi: 10.5505/pajes.2021.53383

[6] Chabok A, van der Aa E, De Hosson JTM, Pei YT. "Mechanical behavior and failure mechanism of resistance spot welded dp1000 dual phase steel" *Materials and Design,* vol. 124, pp. 171–182, 2017.
Doi: 10.1016/j.matdes.2017.03.070

[7] Pouranvari M, Ranjbarnoodeh E. "Resistance spot welding characteristic of ferrite-martensite dp600 dual phase advanced high strength steel-part ii : failure mode" *World Applied Sciences Journal* 15 (11): 1521-1526. 2011

[8] Sung I, Jin M, Cheol D. (2011) "Expulsion Reduction in Resistance Spot Welding by Controlling of welding Current Waveform" *Procedia Engineering*, vol. 10, pp. 2775–2781, Doi: 10.1016/j.proeng.2011.04.461.

[9] Zhang H, Wei A, Qiu X, Chen J. "Microstructure and mechanical properties of resistance spot welded dissimilar thickness DP780/DP600 dual-phase steel joints." *Materials and Design*, vol. 54, pp. 443–449, 2014. doi: http://dx.doi.org/10.1016/j.matdes.2013.08.027.

[10] Zhou K, Cai L. "Study on effect of electrode force on resistance spot welding process" *Journal of Applied Physics,* vol. 116, no. 8, pp. 1–8, 2014
Doi: http://dx.doi.org/10.1063/1.4893968.

[11] Zhao D, Wang Y, Liang D, Zhang P. "Modeling and process analysis of resistance spot welded DP600 joints based on regression analysis" *Materials and Design*, vol. 110, pp. 676–684, 2016
Doi: http://dx.doi.org/10.1016/j.matdes.2016.08.038

[12] Aslanlar S, Ogur A., Ozsarac U, Ilhan E, Demir Z. "Effect of welding current on mechanical properties of galvanized chromided steel sheets in electrical resistance spot welding" *Materials and Design*, vol. 28, no. 1, pp. 2–7, 2007
Doi: 10.1016/j.matdes.2005.06.022.

[13] "Ulsab-Avc," World Auto steel, Adv. Veh. Technol. Program, [Online]. Available: www.ulsab.org, 2002

[14] Safanama DS, Marashi SPH, Pouranvari M. "Similar and dissimilar resistance spot welding of martensitic advanced high strength steel and low carbon steel: metallurgical characteristics and failure mode transition" *Science and Technology of Welding & Joining*, vol. 17, no. 4, pp. 288–294, 2012,
Doi: 10.1179/1362171812Y.0000000006.

[15] Zhang H, Senkara J. Resistance Welding, Fundamentals and Applications, Published in 2006 by CRC Press Taylor & Francis Group, 2006

[16] Rao S. S., Chhibber R., Arora K. S., Shome M., "Resistance spot welding of galvannealed high strength interstitial free steel", *Journal of Materials Processing Technology*, Vol. 246, pp. 252–261, 2017Doi: http://dx.doi.org/10.1016/j.jmatprotec.2017.03.027

[17] Chen N, Wang HP, Carlson BE, Sigler DR, Wang M. "Fracture mechanisms of Al/steel resistance spot welds in coach peel and cross tension testing" *The Journal of Materials Processing Technology*, vol. 252, no. pp. 348–361, 2018
Doi: 10.1016/j.jmatprotec.2017.09.035.

[18] Alizadeh-sh M, Marashi SPH, Pouranvari M. "Resistance spot welding of AISI 430 ferritic stainless steel : Phase transformations and mechanical properties" *Materials and Design*, vol. 56, pp. 258–263, 2014 Doi: 10.1016/j.matdes.2013.11.022.

[19] Long H, Hu Y, Jin X, Shao J, Zhu H. "Effect of holding time on microstructure and mechanical properties of resistance spot welds between low carbon steel and advanced high strength steel" *Computational Materials Science,* vol. 117 pp. 556–563, 2016 Doi: http://dx.doi.org/10.1016/j.commatsci.2016.01.011

[20] Marashi P, Pouranvari M, Amirabdollahian S, Abedi A, Goodarzi M. "Microstructure and failure behavior of dissimilar resistance spot welds between low carbon galvanized and austenitic stainless steels" *Materials Science and Engineering,* v.480 pp.175–80. 2008 Doi:10.1016/j.msea.2007.07.007

[21] Đurić A, Milčić D, Burzić Z, Klobčar D, Milčić M, Marković B, "Microstructure and Fatigue Properties of Resistance Element Welded Joints of DP500 Steel and AW 5754 H22 Aluminum Alloy". *Multidisciplinary Digital Publishing Institute* v.12 pp.258, 20

[22] Chung K, Noh W, Yang X, Han HN, Lee MG. "Practical failure analysis of resistance spot welded advanced high-strength steel sheets" *International Journal of Plasticity* v.94, pp.122–147, 2017.Doi: 10.1016/j.ijplas.2016.10.010.